DOI:10.1093/jnci/djt373

ARTICLE

Role of Oncogenic K-Ras in Cancer Stem Cell Activation by Aberrant Wnt/β-Catenin Signaling

Byoung-San Moon, Woo-Jeong Jeong, Jieun Park, Tae Il Kim, Do Sik Min, Kang-Yell Choi

Manuscript received July 22, 2013; revised November 11, 2013; accepted November 14, 2013.

Correspondence to: Kang-Yell Choi, PhD, Department of Biotechnology; Translational Research Center for Protein Function Control, Yonsei University, Seoul, 120–749, Korea (e-mail: kychoi@yonsei.ac.kr).

Background Adenomatous polyposis coli (*APC*) loss-of-function mutations and *K-Ras* gain-of-function mutations are common abnormalities that occur during the initiation and intermediate adenoma stages of colorectal tumorigenesis, respectively. However, little is known about the role these mutations play in cancer stem cells (CSCs) associated with colorectal cancer (CRC) tumorigenesis.

Methods We analyzed tissue from CRC patients (n = 49) to determine whether *K-Ras* mutations contributed to CSC activation during colorectal tumorigenesis. DLD-1-K-Ras-WT and DLD-1-K-Ras-MT cells were cultured and evaluated for their ability to differentiate, form spheroids in vitro, and form tumors in vivo. Interaction between *APC* and *K-Ras* mutations in colorectal tumorigenesis was evaluated using $APC^{Min/+}$/$K\text{-}Ras^{LA2}$ mice and DLD-1-K-Ras-WT and DLD-1-K-Ras-MT cell xenografts. (n = 4) Group differences were determined by Student *t* test. All statistical tests were two-sided.

Results The sphere-forming capability of DLD-1-K-Ras-MT cells was statistically significantly higher than that of DLD-1-K-Ras-WT cells (DLD-1-K-Ras-MT mean = 86.661 pixel, 95% confidence interval [CI] = 81.701 to 91.621 pixel; DLD-1-K-Ras-WT mean = 42.367 pixel, 95% CI = 36.467 to 48.267 pixel; $P = .003$). Moreover, both the size and weight of tumors from DLD-1-K-Ras-MT xenografts were markedly increased compared with tumors from DLD-1-K-Ras-WT cells. Expression of the CSC markers CD44, CD133, and CD166 was induced in intestinal tumors from $APC^{Min/+}$/$K\text{-}Ras^{LA2}$mice, but not $K\text{-}Ras^{LA2}$ mice, indicating that *APC* mutation is required for CSC activation by oncogenic *K-Ras* mutation.

Conclusions *K-Ras* mutation activates CSCs, contributing to colorectal tumorigenesis and metastasis in CRC cells harboring *APC* mutations. Initial activation of β-catenin by *APC* loss and further enhancement through *K-Ras* mutation induces CD44, CD133, and CD166 expression.

JNCI J Natl Cancer Inst (2014) 106(2): djt373 doi:10.1093/jnci/djt373

Colorectal cancer (CRC) is one of the most common cancers worldwide, and approximately 50% of patients with CRC develop liver metastases (1). Although cancer stem cells (CSCs) represent a small subpopulation of the tumor cells, they play important roles in the development of primary and metastatic CRC (2–4). Cell surface markers such as CD44, CD133, and CD166 have been used for identification of CSCs (5–7). Adenomatous polyposis coli (*APC*) loss-of-function and *K-Ras* gain-of-function mutations are both common abnormalities in CRC that occur during the initiation and intermediate adenoma stages of colorectal tumorigenesis, respectively (8,9). However, little is known about the role of these mutations in the regulation of CSCs associated with the tumorigenesis of CRC.

The Wnt/β-catenin pathway is involved in cell differentiation, proliferation, and motility. Activation of this pathway is determined by stabilization and nuclear accumulation of β-catenin and subsequent transcriptional activation of Wnt target genes (10–12). The Wnt/β-catenin pathway is also known to be involved in the maintenance of homeostasis of intestinal stem cells and crypt cells (13,14) and several CSC markers, such as CD44 and CD133, and leucine-rich repeats containing G protein-coupled receptor 5 (Lgr5) are known transcriptional targets of Wnt/β-catenin signaling (15,16).

K-Ras acts as a molecular switch to regulate the extracellular signal-regulated kinase (ERK) and phosphatidyl inositol 3-kinase (PI3K)–Akt signaling pathways, and mutations fixing K-Ras in its GTP-bound active forms are found in approximately 40% of human CRCs (17,18). *K-Ras* mutations occur during the progression and metastasis of CRCs, processes that also involve CSC (19–21).

Because we initially observed an association between *K-Ras* mutations and CSC marker expression in CRC patients, we systematically investigated the relationship between *K-Ras* mutation and CSC activation in colorectal tumorigenesis. The activation of CSCs and the subsequent neoplastic growth of tumors were enhanced by oncogenic *K-Ras* mutation in the genetic background

of *APC* loss. Such an outcome could be achieved by the enhanced activation of Wnt/β-catenin signaling. CSC activation by aberrancies in both the Wnt/β-catenin and Ras/ERK pathways provides a new perspective on genetic interaction between *APC* and *K-Ras* mutations in colorectal tumorigenesis.

Methods

Patient Tissues, Mice, Tissue Preparation

Human colon tissues (Supplementary Table 1, available online) were obtained from 49 patients in accordance with ethical standards of Severance Hospital on human experimentation, and all patients gave written informed consent. *K-Ras* mutational analyses were performed as described previously (22). All animal experiments were performed in accordance with the Korean Food and Drug Administration guidelines. Protocols were reviewed and approved by the Institutional Animal Care and Use Committee of the Yonsei Laboratory Animal Research Center. For xenograft assays, BalbC/nude and Nod/Scid mice were purchased from the Central Lab Animal Inc. (Seoul, Korea). The C57BL6J-*APC*$^{Min/+}$, C57BL6J-*K-Ras*^{LA2}, and wild-type C57BL6J mice were purchased from Jackson Laboratory (Bar Harbor, ME), and *APC*$^{Min/+}$ and *K-Ras*^{LA2} double mutant mice were generated by crossing C57BL6J-*APC*$^{Min/+}$ with C57BL6J-*K-Ras*^{LA2} mice. For tissue preparation, intestinal specimens from 12-week-old C57BL6J, *APC*$^{Min/+}$, *K-Ras*^{LA2}, and *APC*$^{Min/+}$/*K-Ras*^{LA2} mice were processed immediately after the mice were killed.

In Vitro Differentiation Assay and Alkaline Phosphatase Staining

For in vitro differentiation, small spheres were plated in 0.1% gelatin-coated plates and Roswell Park Memorial Institute medium containing 5% fetal bovine serum was layered on top. Differentiation kinetics were evaluated over 3 days by measuring the size and number of spheres and quantified as described previously (23) using WCIF ImageJ bundle software v1.37a (University Health Network Research, Toronto, Canada). To measure intestinal alkaline phosphatase activity, we used Alkaline Phosphatase Substrate Kit 1 (SK-5100) from Vector Laboratories (Burlingame, CA) according to the manufacturer's instructions. Quantification was performed with a general optical microscope (TE-200U; Nikon, Tokyo, Japan).

In Vivo Xenotransplantation, Metastasis, and Imaging Analyses

After acclimatization for 1 week, 1 × 10^6 D-K-Ras-WT or MT cells in 200 μL phosphate-buffered saline/Matrigel (1:1) were subcutaneously injected into the dorsal flank of athymic nude mice (n = 4 mice per group). Tumor volume and body weight of mice were measured every 3 days. Tumor volumes were measured using Verniar calipers, applying the formula π/6 × length × width × height. Body weights of mice were measured using an electronic balance at 3 and 6 weeks. Tumor burdens in the liver or lung of nude mice were monitored 8 weeks after intrasplenic injection with 5 × 10^5 D-K-Ras-WT (n = 8) or –MT (n = 12) cells in 50 μL phosphate-buffered saline/Matrigel (1:1). Tumors were excised, weighed, and fixed in 4% paraformaldehyde for further analysis. For in vivo imaging, fluorescent magnetic nanoparticles consisting of a magnetic core and silica-shell encapsulating fluorescent organic dyes of NIR675 (Biterials, Seoul, Korea) were mixed with medium. RKO cells were mixed with or without (negative control) the nanoparticle mixture and incubated for 16 hours to allow insertion by endocytosis. The nanoparticle-inserted cells were transfected with plasmids by electrophoration, and trypsinized cells were injected into subcutaneous regions of nude mice. The mice were then subjected to imaging analyses on a Kodak In-Vivo Multispectral Imaging System (Carestream Health, New Haven, CT) with excitation at 675 nm and emission at 700 nm. Fluorescence data were collected for 3 minutes on a 4- megapixel camera using 4 × 4 binning. Sixteen-bit images were exported, and quantification of fluorescence intensity or area was performed using WCIF ImageJ bundle software v1.37a.

Statistical Analyses

All statistical analyses and calculations were performed using Microsoft Excel spreadsheets and GraphPad Prism v.6 (GraphPad Software, La Jolla, CA). Group differences were determined with the Student *t* test. Data are expressed as means and standard deviation or 95% confidence intervals (CIs). All statistical tests were two-sided, and *P* values less than .05 were considered statistically significant. Additional methods are available in the Supplementary Methods (available online).

Results

Influence of Oncogenic *K-Ras* Mutation on CSC Characteristics of CRC Cells Carrying Mutant *APC*

To identify any involvement of *K-Ras* mutation in the activation of CSCs during colorectal tumorigenesis, we tested human CRC patient tissues (n = 49) (Supplementary Table 1, available online). We identified *K-Ras* mutations in 14 of 49 (29%) patient CRC specimens by DNA sequencing analyses. Total expression levels of CD44, CD133, and CD166 CSC markers and nuclear localized β-catenin, which were obtained through quantitative tissue fluorescence activated cell sorting analyses, were higher in tissues carrying *K-Ras* mutation than in those with wild-type *K-Ras*. The expression levels of the CSC markers were higher in metastatic liver cancers compared with early stages (Supplementary Figure 1C, available online).

To investigate the role of *K-Ras* mutation in the activation of intestinal CSCs in CRCs, we used *APC* mutant isogenic D-K-Ras-WT and D-K-Ras-MT cells harboring wild-type and mutant *K-Ras*, respectively (24). After 7 days of culture, the sphere-forming capability of D-K-Ras-MT cells was higher than that of D-K-Ras-WT cells (2000 cells seeded; DLD-1-K-Ras-MT mean = 86.661 pixel, 95% confidence interval [CI] = 81.701 to 91.621 pixel; DLD-1-K-Ras-WT mean = 42.367 pixel, 95% CI = 36.467 to 48.267 pixel; *P* = .003) (Figure 1, A and B). The subpopulation of cells showing a triple-positive phenotype for CD44, CD133, and CD166 CSC markers was 2.6-fold higher in spheres formed by D-K-Ras-MT cells compared with those formed by D-K-Ras-WT cells (Figure 1C). The high expression levels of CD44, CD133, and CD166 in the spheres derived from D-K-Ras-MT cells were confirmed by immunofluorescent staining of single cells derived from spheres using Amnis imaging fluorescence activated cell sorting (Figure 1D) and by immunocytochemical staining of the spheres (Figure 1E). When

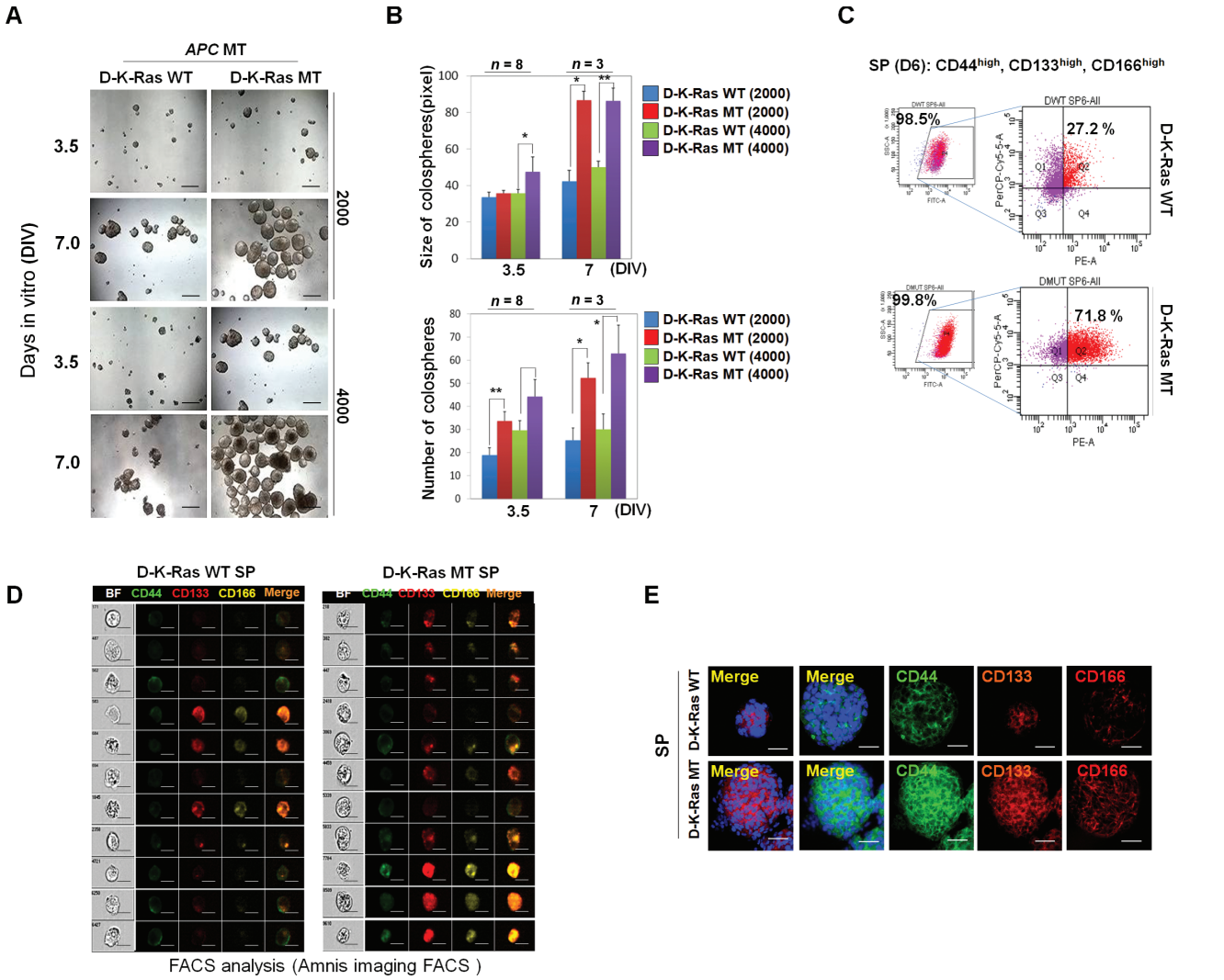

Figure 1. Effects of oncogenic *K-Ras* mutation on sphere (SP) formation of colorectal cancer (CRC) cells carrying an *APC* mutation. **A** and **B**) D-K-Ras-WT or D-K-Ras-MT cells were seeded at a density of 2×10^3 (n = 8) or 4×10^3 (n = 3) cells/plate in ultra-low attachment 96-well plates for 3.5 or 7 days to allow SP formation. **B**) Relative sizes and numbers of SPs in (**A**) were measured and quantified as described in the Supplementary Methods (available online). Two-sided Student *t* test was used to determine statistical significance. Error bars represent 95% confidence intervals. (n = 3). $*P < .05$, $**P < .005$. Scale bar = 250 μm. DIV = days in vitro. **C**) Fluorescence activated cell sorting (FACS) analyses of CD44, CD133, and CD166 triple-positive suspended cells. **D**) Merged images of the CD44, CD133, CD166 triple-positive subpopulation among single cells derived from SP forms of D-K-Ras-WT or D-K-Ras-MT cells. Scale bar = 10 μm. **E**) Immunocytochemical analyses of CD44, CD133, and CD166. Cells were counter-stained with 4′,6-diamidino-2-phenylindole (DAPI). Images were captured using a Zeiss confocal microscope. Scale bar = 50 μm.

comparing the secondary sphere-forming abilities of D-K-Ras-WT and D-K-Ras-MT cells, high population of CD44/CD133/CD166 triple positive ($CD44^{high}CD133^{high}$ $CD166^{high}$) cells (n = 3–6) was higher; in particular, cells obtained from D-K-Ras-MT cells showed higher sphere-forming ability than those derived from D-K-Ras-WT cells ($CD44^{low}CD133^{low}CD166^{low}$ DLD-1-K-Ras-MT cells = 4.509 pixel, 95% CI = 1.77 to 7.248 pixel; vs $CD44^{high}CD133^{high}$ $CD166^{high}$ cells = 10 pixel, 95% CI = 5.382 to 14.617 pixel; $P = .002$) (Figure 2, A and B). The secondary sphere-forming abilities of $CD133^{high}$ cells showed similar dependency on *K-Ras* status (colosphere size and number of DLD-1-K-Ras-MT cells; two-sided *t* test, $P < .05$) (Supplementary Figure 2, A and B, available online).

The mRNA levels of Oct4, Nanog, and Sox2 pluripotency markers were higher (30%–40%) in the spheres derived from D-K-Ras-MT cells (two-sided *t* test, $P < .05$) (Supplementary Figure 2C, available online). We also tested the differentiation potential of the spheres by observing their morphological changes (25). The differentiation rate of spheres derived from D-K-Ras-MT cells was lower than that derived from D-K-Ras-WT cells as revealed by cell morphology and positive alkaline phosphatase staining (relative 2 or 3 day differentiation; ie, extent of undifferentiated multilayer sphere morphology) (Figure 2C; Supplementary Figure 2D, available online). Maintenance of an undifferentiated status of the spheres derived from D-K-Ras-MT cells was revealed by weak expression of the gastrointestinal differentiation marker CK20 (Figure 2D). Upon induction of differentiation, CD44, CD133, and CD166 expression persisted in the spheres derived from D-K-Ras-MT cells but was mostly abolished in those derived from D-K-Ras-WT cells (Figure 2D). Because CSCs are hypothesized to be chemoresistant, we investigated the effect of 5-fluorouracil (5-FU), a commonly used drug for the treatment of CRC, on the viability of D-K-Ras-WT and D-K-Ras-MT cells (n = 3). D-K-Ras-MT cells,

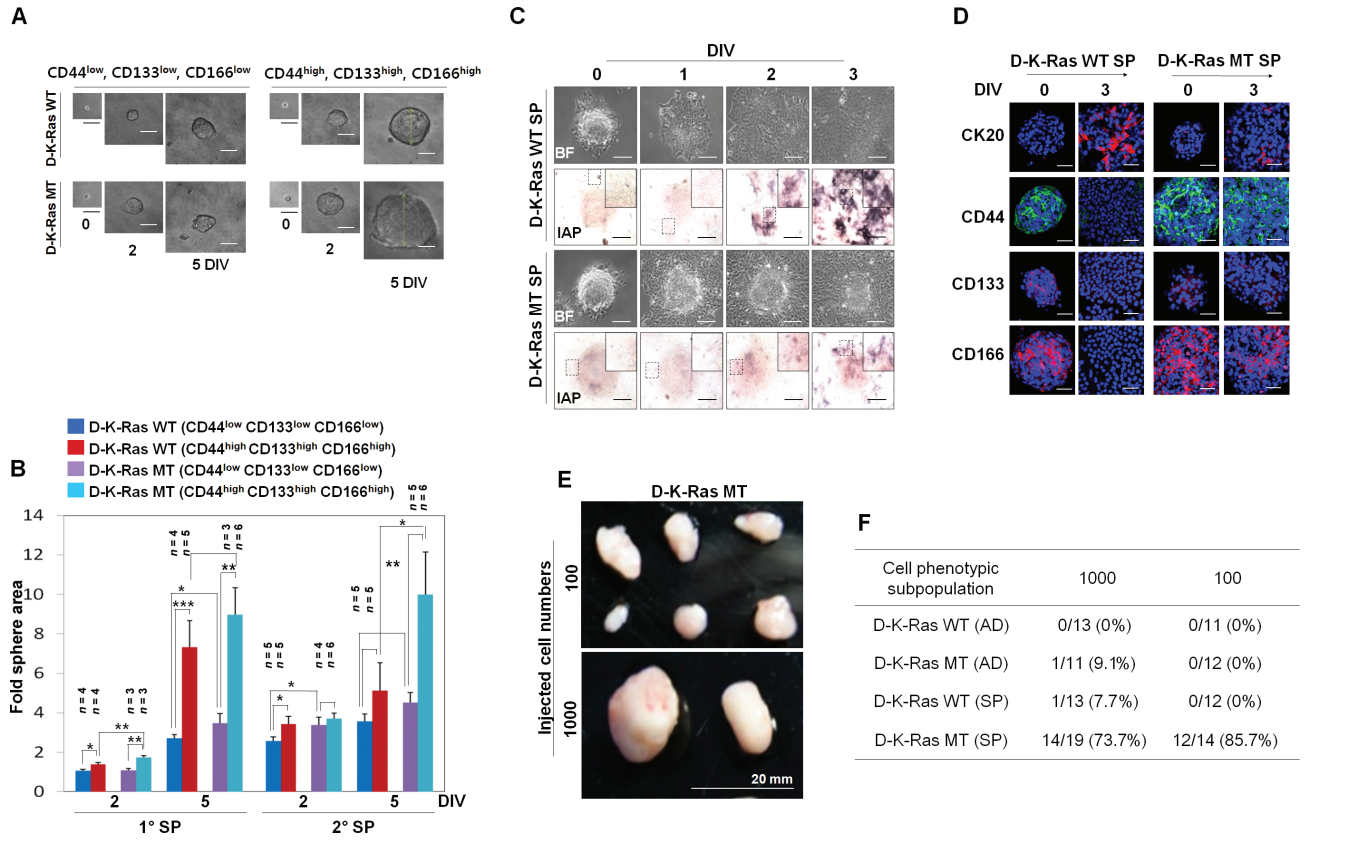

Cell phenotypic subpopulation	1000	100
D-K-Ras WT (AD)	0/13 (0%)	0/11 (0%)
D-K-Ras MT (AD)	1/11 (9.1%)	0/12 (0%)
D-K-Ras WT (SP)	1/13 (7.7%)	0/12 (0%)
D-K-Ras MT (SP)	14/19 (73.7%)	12/14 (85.7%)

Figure 2. Effect of oncogenic *K-Ras* mutation on self-renewal, differentiation, and tumorigenic potential of colorectal cancer cells carrying an *APC* mutation. **A** and **B**) D-K-Ras-WT and D-K-Ras-MT cells were cultured as sphere (SP) forms. CD44^{high} CD133^{high} CD166^{high} and CD44^{low} CD133^{low} CD166^{low} cells were sorted from dissociated SP cells at a purity of 99.8% by fluorescence activated cell sorting (FACS). **A**) Single cells of triple-low or -high populations of D-K-Ras-WT or D-K-Ras-MT were separated by serial dilution and SP formation was induced for 5 days in vitro (DIV). Scale bar = 50 μm. **B**) Quantification of relative sizes of primary or secondary SPs in (**A**).Two-sided Student *t* test was used to determine statistical significance. Error bars represent 95% confidence intervals (CIs). (n = 3–6). **P* < .05, ***P* < .005, ****P* < .0005. **C**) SPs of D-K-Ras-WT or D-K-Ras-MT cells were grown and differentiation capabilities were monitored by changes in morphology (**upper panel**) and intestinal alkaline phosphatase (IAP) staining (**lower panel**). Scale bar = 50 μm. **D**) D-K-Ras-WT or D-K-Ras-MT SPs were subjected to immunofluorescent labeling using antibodies specific for cytokeratin (CK)–20, CD44, CD133, or CD166. Nuclei were counter stained with 4′,6-diamidino-2-phenylindole (DAPI). Scale bar = 50 μm. **E** and **F**) Cells from the indicated populations were injected into NOD/SCID mice. **E**) Images of tumors isolated from NOD/SCID mice injected with D-K-Ras-MT cells. Scale bar = 20 mm. **F**) The number of tumors for each condition are presented. (**A**) and (**C**) were captured as B/W images using a *Ti*-Nikon fluorescence microscope.

especially sphere-forming cells, were more resistant to 5-FU than D-K-Ras-WT cells (Supplementary Figure 2E, available online). In addition, the level of apoptosis of D-K-Ras-MT cells was lower in cells that formed spheres than in adherent cells (Supplementary Figure 2F, available online).

To compare CSC characteristics, different numbers of adherent and sphere-forming cells were injected into severe combined immunodeficient (SCID) mice (6) and tumor-forming capacity was measured (Figure 2, E and F; Supplementary Figure 3A, available online). The tumor-forming capacity of D-K-Ras-MT cells, especially those derived from spheroids, was markedly higher than that of D-K-Ras-WT cells derived from spheroids, which only formed tumors at low frequencies with large numbers of cells (1×10^3) (Figure 2F). We also observed dose-dependent secondary tumor formation after injecting cells isolated from primary tumors induced by D-K-Ras-MT cells. The histological characteristics of those tumor tissues were similar (Supplementary Figure 3B, available online). Overall, oncogenic *K-Ras* increased CSC characteristics of CRC cells carrying *APC* mutation both in vitro and in vivo.

Effect of CSC Activation by *K-Ras* Mutation in CRCs Carrying *APC* Mutation on Tumor Growth in a Mouse Xenograft Model

To investigate the association between *K-Ras* mutation and CSC activation in vivo, we performed mice xenograft studies using D-K-Ras-WT and D-K-Ras-MT cells. Both the volume (DLD-1-K-Ras-MT cells = 406.214 mm^3, 95% CI = 332.603 to 479.825 mm^3; vs DLD-1-K-Ras-WT cells = 20.977 mm^3, 95% CI = 12.273 to 29.681 mm^3; $P < .0001$) and weight of tumors (DLD-1-K-Ras-MT cells = 0.743 g, 95% CI = 0.622 to 0.865 g; vs DLD-1-K-Ras-WT cells = 0.046 g, 95% CI = 0.023 to 0.068 g; $P = .0001$) as well as the expression levels of CD44, CD133, and CD166 were markedly increased in mouse xenografts with D-K-Ras-MT cells compared with those with D-K-Ras-WT cells (Figure 3, A–C; Supplementary Figure 4, A and B, available online). Interestingly, we observed increased staining intensity of both total and nuclear β-catenin in D-K-Ras-MT cells (Figure 3C). Both the size (si-K-Ras = 34.667 pixel, 95% CI = 32.938 to 36.395 pixel; vs si-control = 104.667 pixel, 95% CI = 85.253 to 124.08 pixel; $P = .022$) and number (especially of large

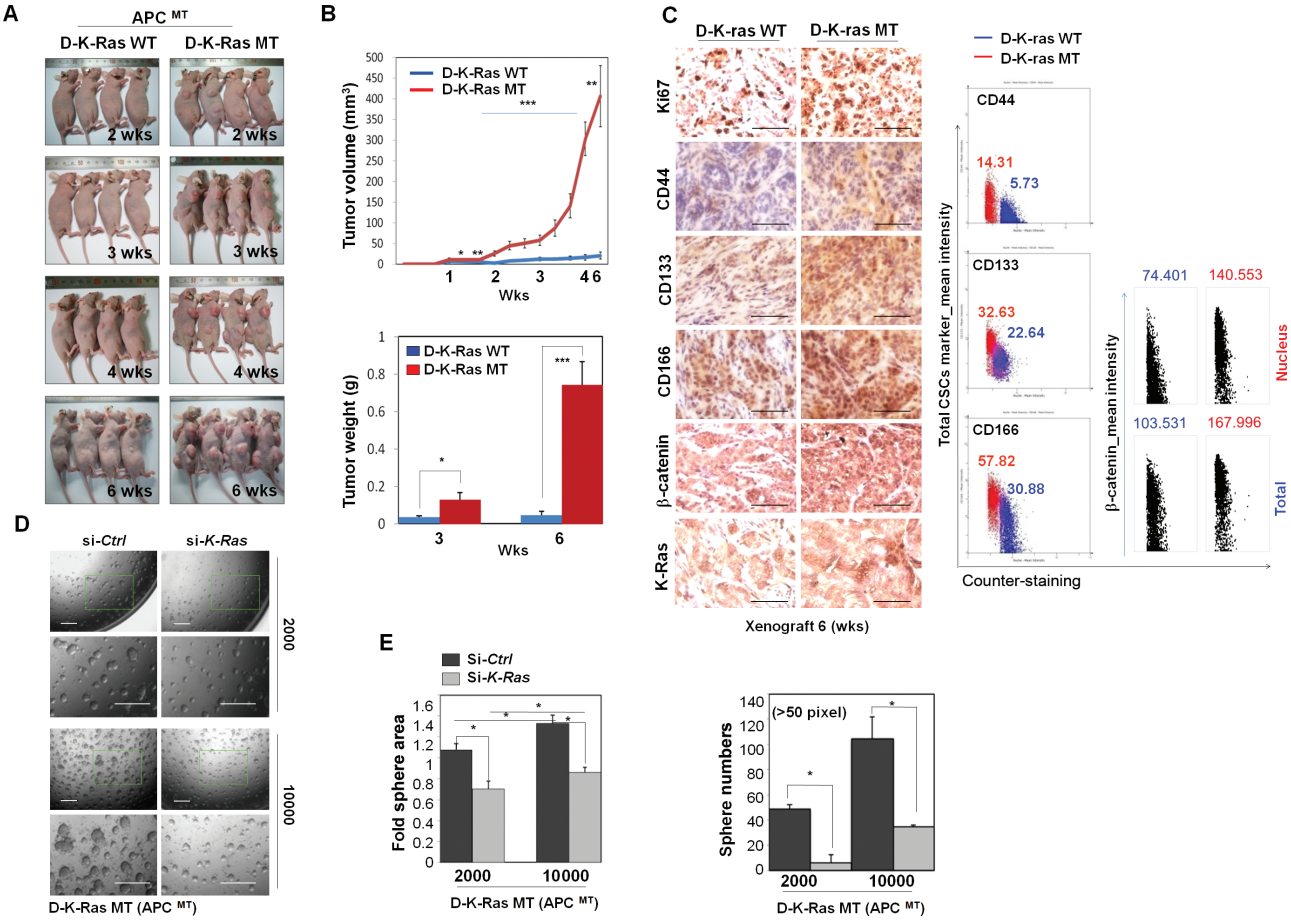

Figure 3. Influence of oncogenic *K-Ras* on xenograft tumor growth and cancer stem cell (CSC) marker expression in colorectal cancer (CRC) cells carrying *APC* mutations in vivo and in vitro. **A** and **B**) D-K-Ras-WT or D-K-Ras-MT cells (5×10^6 each) were injected subcutaneously into the flanks of nude mice (n = 4 per group). **A**) Representative gross images of mice. **B**) Tumor volume (**upper panel**) was measured every 3 days, and tumor weight (**lower panel**) was measured after mice were killed at 3 or 6 weeks. Two-sided Student *t* test was used to determine statistical significance. Error bars represent 95% confidence intervals. (n = 4). $*P < .05$, $**P < .005$, $***P < .0005$. **C**) Paraformaldehyde (PFA)-fixed paraffin sections from 6-week-old xenograft mice were incubated with antibodies against Ki-67, CD44, CD133, CD166, β-catenin, or K-Ras and stained with 3,3′-diaminobenzidine (DAB). The expression of CD44, CD133, CD166, β-catenin, and nuclear β-catenin in CRC tissues was quantified using Histo Quest software. Scale bar = 200 μm. **D**) D-K-Ras-MT (2×10^3 or 1×10^4) cells electroporated with control or K-Ras small interfering RNA were grown on ultra-low attachment 96-well plates for up to 6 days. Scale bar = 250 μm. **E**) Quantification of relative size and number of spheres in (**D**). Data are shown as mean ± standard deviation (n = 3). $*P < .05$, two-sided Student *t* test.

spheres) of spheres derived from D-K-Ras-MT cells were statistically significantly reduced by knockdown of oncogenic K-Ras (si-K-Ras = 0.862 pixel, 95% CI = 0.809 to 0.916 pixel; vs si-control = 1.327 pixel, 95% CI = 1.235 to 1.420 pixel; $P = .007$) (Figure 3, D and E). The role of oncogenic *K-Ras* in the activation of CSCs was also revealed by observing the increased expression levels of CSC markers in cells expressing green fluorescent protein (EGFP)–fused oncogenic K-Ras (EGFP-K-Ras^{V12}) compared with those in cells expressing EGFP in D-K-Ras-WT cells (Supplementary Figure 4C, available online).

Effect of *APC* Loss on Initiation and Malignant Progression of Tumors Involving Activation of CSCs by *K-Ras* Mutation

We further investigated the interaction between *APC* and *K-Ras* mutations in the activation of CSCs and tumorigenesis using $APC^{Min/+}$ mice and $K\text{-}Ras^{LA2}$ transgenic mice. $APC^{Min/+}$ mice, but not $K\text{-}Ras^{LA2}$, mice formed obvious tumors in the small intestinal crypts. However, the tumor incidence, especially that of large tumors, was critically increased in $APC^{Min/+}/K\text{-}Ras^{LA2}$ double-mutant mice ($APC^{Min/+}/K\text{-}Ras^{LA2}$ = 51, 95% CI = 22.117 to 79.883; vs $APC^{Min/+}$ = 14.667, 95% CI = 5.950 to 23.383; $P = .02$) (Figure 4A; Supplementary Figure 5, A and B, available online). The expression levels of the CSC markers and β-catenin in the nuclei were higher in tumors from $APC^{Min/+}/K\text{-}Ras^{LA2}$ mice than those from $APC^{Min/+}$ or $K\text{-}Ras^{LA2}$ mice (Figure 4B; Supplementary Figure 5, C–E, available online). Therefore, induction of CSC markers by *K-Ras* mutation requires the additional *APC* mutation. The enhanced activation of Wnt/β-catenin signaling was also confirmed in vitro by observing increased β-catenin nuclear localization in D-K-Ras-MT cells that formed spheres compared with adherent cells and in D-K-Ras-WT cells expressing EGFP-K-Ras^{V12} (Supplementary Figure 6, A–C, available online).

Next, we measured the effects of the overexpression of GFP-tagged truncated APC (EGFP-$APC^{1\text{-}777}$) and/or EGFP-K-Ras^{V12} on sphere-forming abilities of RKO cells harboring wild-type *APC* and *K-Ras*. The size of spheres was slightly increased by the overexpression of EGFP-$APC^{1\text{-}777}$ but was markedly increased by the coexpression of both EGFP-$APC^{1\text{-}777}$ and EGFP-K-Ras^{V12}

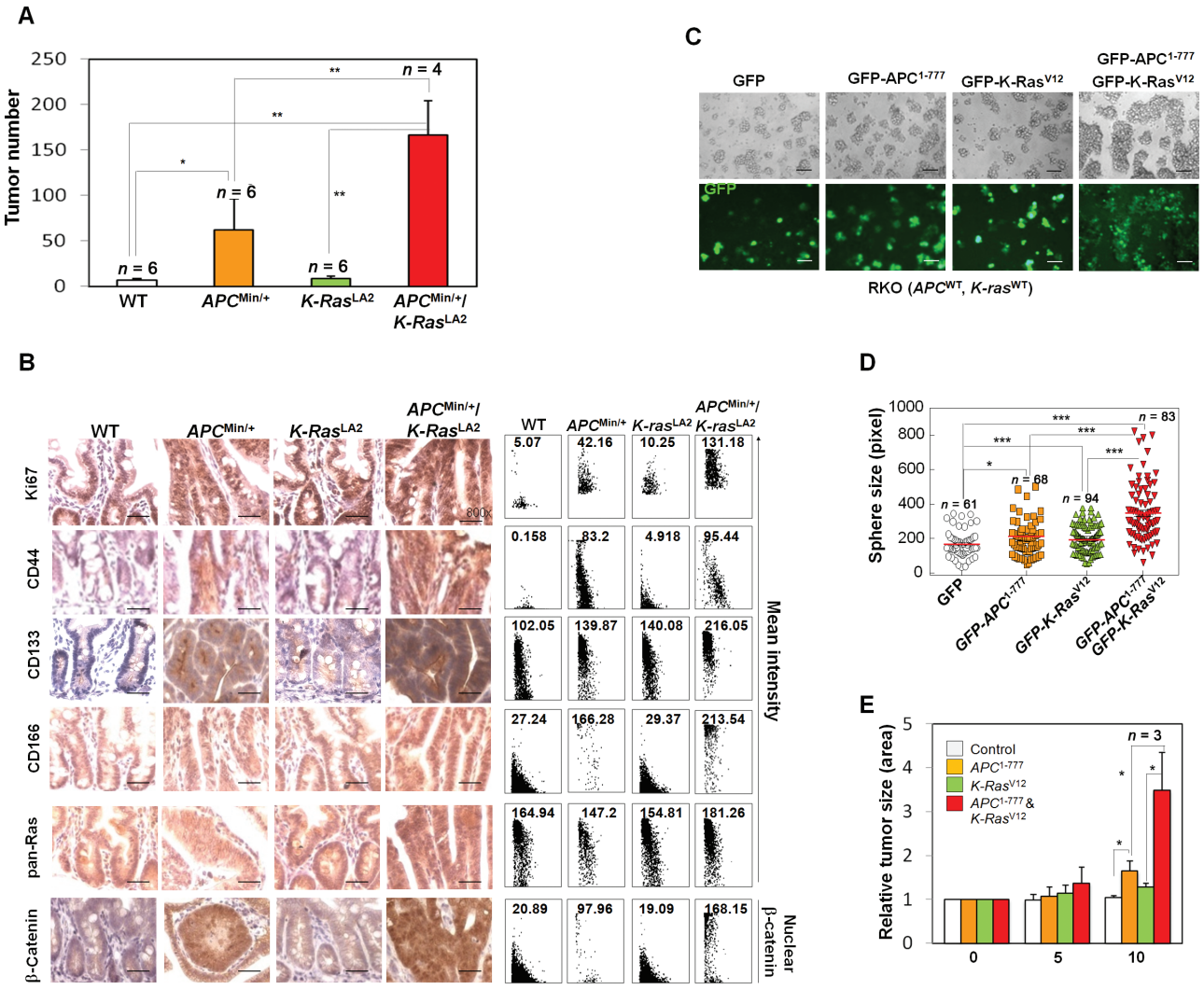

Figure 4. Primary mutation of *APC* is required for oncogenic *K-Ras* to activate cancer stem cells and enhance tumorigenic potential. **A** and **B**) Wild-type (WT; n = 6), *APC*$^{Min/+}$ (n = 6), *K-Ras*^{LA2} (n = 6), or *APC*$^{Min/+}$/*K-Ras*^{LA2} (n = 4) mice were killed at 12 weeks. Tissues were prepared as described in the Supplementary Methods (available online), and the **d**issected small intestine was stained with methylene blue and captured by an optical camera (Supplementary Figure 5A, available online). **A**) The total number of polyps was counted in the whole intestine from at least four different mice. Two-sided Student *t* test was used to determine statistical significance. Error bars represent 95% confidence intervals (CIs). **P* < .05, ***P* < .005. **B**) Paraformaldehyde (PFA)-fixed paraffin sections from intestinal tumor tissues of *APC*$^{Min/+}$, *K-Ras*^{LA2}, and *APC*$^{Min/+}$/*K-Ras*^{LA2} mice were incubated with antibodies against Ki67, CD44, CD133, CD166, β-catenin, or pan-Ras and subjected to 3,3′-diaminobenzidine (DAB) immunohistochemical staining. Representative images were selected from at least three different fields. The expressions of total Ki67, CD44, CD133, CD166, nuclear β-catenin, and pan-Ras were quantified using Histo Quest software. Scale bar = 50 μm. **C**) RKO cells were electroporated with 2 μg EGFP-control, EGFP-*APC*$^{1-777}$, EGFP-*K-Ras*^{V12}, or both EGFP-*APC*$^{1-777}$ and EGFP-*K-Ras*^{V12} vectors using Amaxa Nucleofector. Transfected cells were grown on ultra-low attachment 96-well plates (2×10^3 cells/well) for up to 7 days. Images were captured as B/W (**upper**) and fluorescent (**lower**) images using a *Ti* Nikon fluorescence microscope. Scale bar = 100 μm. GFP = green fluorescent protein. **D**) The relative sizes of spheres from (**C**) were quantified by Image J quantification software (EGFP-APC$^{1-777}$/EGFP-K-Ras^{V12} RKO mean = 347.675 pixel, 95% CI = 311.717 to 383.632 pixel; vs EGFP-*APC*$^{1-777}$ mean= 202.235 pixel, 95% CI = 179.132 to 225.339 pixel; *P* < .0001). **E**) Transfected RKO cells (5×10^5) containing nanoparticles (NEO-LIVE™-Magnoxide 675) were transplanted into a subcutaneous region of BalbC/nude mice (n = 3 each) and grown for 15 days (Supplementary Figure 7, A and B, available online). Relative tumor sizes were estimated by measuring the tumor size on captured images at 0, 5, or 10 days using Image J quantification software. Two-sided Student *t* test was used to determine statistical significance. Error bars represent 95% confidence intervals. **P* < .05, ***P* < .005, ****P* < .0005, two-sided *t* test.

(Figure 4, C and D). In vivo imaging analyses of mouse xenografts showed that the relative growth rate of EGFP-*APC*$^{1-777}$/EGFP-*K-Ras*^{V12}–expressing tumors was much higher than those expressing either EGFP-*APC*$^{1-777}$ or EGFP-*K-Ras*^{V12} alone (EGFP-APC$^{1-777}$/EGFP-K-Ras^{V12} = 3.308 pixel, 95% CI = 1.956 to 4.660 pixel; vs EGFP-*APC*$^{1-777}$ = 1.650 pixel; 95% CI = 1.428 to 1.872 pixel; *P* = .03) (Figure 4E; Supplementary Figure 7, A and B, available online).

Effect of Oncogenic K-Ras on CSCs by Activation of the Wnt/β-Catenin Signaling Pathway Through ERK

We tested the involvement of downstream ERK in the activation of Wnt/β-catenin signaling and CSC characteristics by monitoring the effects of AS703026, a specific MEK inhibitor (26). We found that the self-renewal of D-K-Ras-MT cells was reduced by AS703026 treatment (n = 3; *t* test, *P* < .005) (Figure 5, A and B). In addition, mRNA levels of CD44,

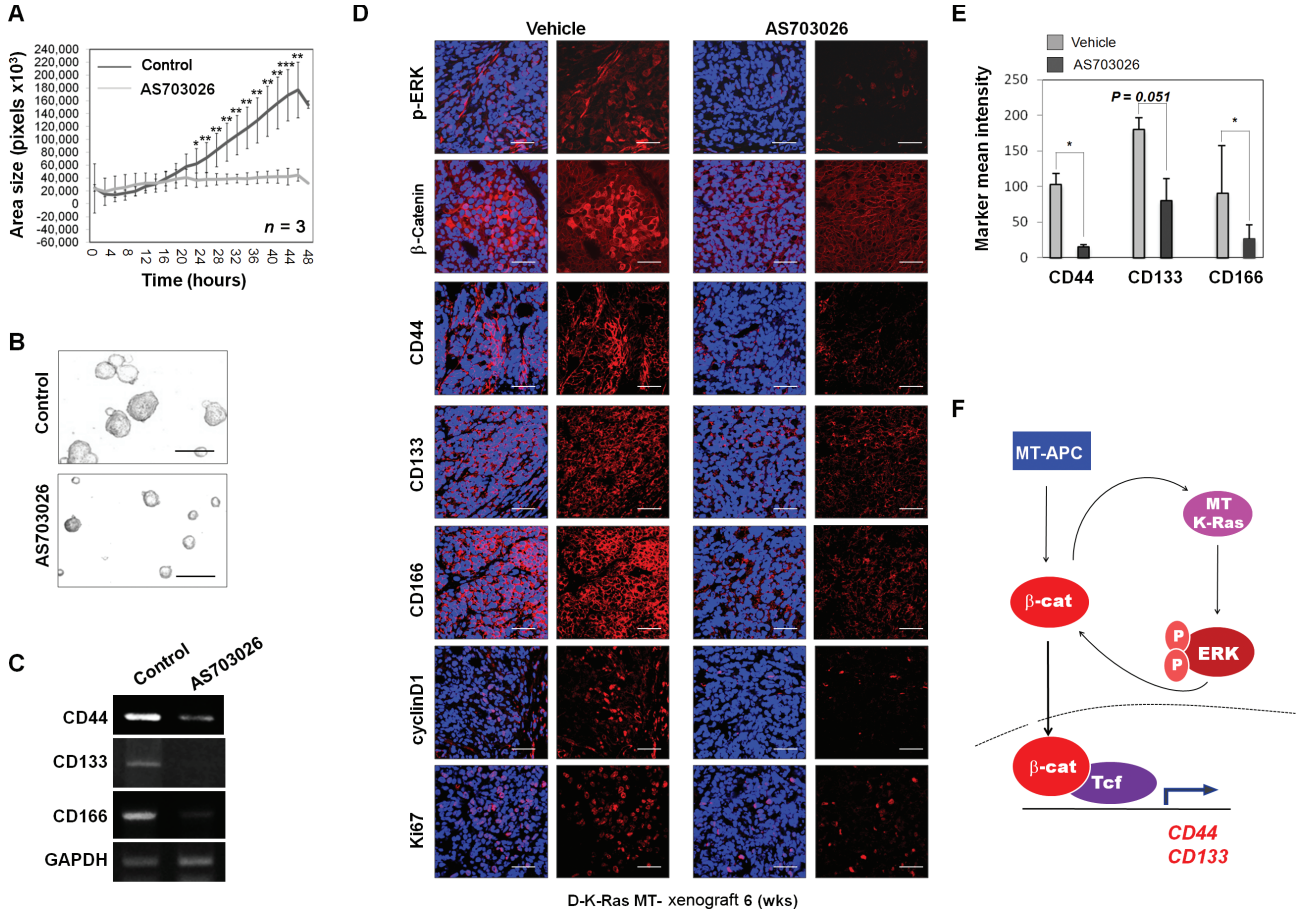

Figure 5. Cancer stem cell activation by oncogenic K-Ras occurs by enhanced β-catenin activation through ERK by loss of *APC*. **A**) Sphere formation of D-K-Ras-MT cells after treatment with 200 nM AS703026 was monitored in real time as described in the Supplementary Methods (available online). Data are shown as mean ± standard deviation. $*P < .05$, $**P < .005$, $***P < .0005$, two-sided *t* test. **B**) Representative B/W images for data in (**A**). Scale bar = 100 μm. **C**) D-K-Ras-MT cells treated with 200 nM AS703026 were grown on 6-well plates (5×10^4 cells/plate) for up to 6 days. Reverse-transcription polymerase chain reaction analyses were performed to detect *CD44, CD133, CD166,* or *GAPDH* mRNA. **D**) D-K-Ras-MT cells (5×10^6 each) were injected subcutaneously into the flanks of athymic nude mice. When the average tumor volume was 200 mm^3, mice was treated for 28 days by oral gavage with vehicle (0.5% methyl cellulose and 0.4% Tween 80) or 10 mg/kg AS703026 once daily. Paraformaldehyde (PFA)-fixed paraffin sections from xenograft mice were subjected to immunofluorescent labeling using antibodies specific for p-ERK, β-catenin, CD44, CD133, CD166, cyclin D1, or Ki-67. Nuclei were counter stained with 4′,6-diamidino-2-phenylindole (DAPI) . Representative images were selected from at least three different fields. Scale bar = 50 μm. **E**) The expression of total CD44, CD133, and CD166 was quantified data using Histo Quest software. Data are shown as mean ± standard deviation. $*P < .05$, two-sided *t* test. **F**) A model for cancer stem cell activation by *K-Ras* mutation in colorectal cancer cells carrying *APC* mutations. Initial activation of β-catenin by *APC* loss and further enhancement through K-Ras mutation induce CD44 and CD133 expression by β-catenin and Tcf mediated transcriptional activation. See also Figure 6D.

CD133, and CD166 (Figure 5C) and protein levels of all the CSC markers as well as β-catenin and its target cyclin D1 (Supplementary Figure 8, available online) were reduced by AS703026 in the sphere-forming D-K-Ras-MT cells. The role of MEK inhibitor in the inhibition of Wnt/β-catenin signaling during CSC activation in vivo was shown by measuring the effects of AS703026 on the tumors generated by xenografts with D-K-Ras-MT cells (Figure 5, D and E). We analyzed microarray data from human CRC specimens with wild-type (n = 7) or mutant (n = 7) *APC* that also carried either *K-Ras* or *B-Raf* mutations (Supplementary Figure 9, A and B, available online). This analysis revealed that the mRNA levels of CSC markers were all increased in patient tissues with mutant *APC* (Supplementary Figure 9, C–E, available online). Overall, these data show that activation of the ERK pathway by oncogenic *K-Ras* induces CSC marker expressions in CRC cells by activation of Wnt/β-catenin signaling (Figure 5F).

Role of Oncogenic *K-Ras* in Liver Metastasis of CRC Cells Harboring *APC* Mutation

The oncogenic *K-Ras* mutation has been shown to be involved in the metastatic progression of human CRC to the liver (20), but the process has been questioned (27,28). We found that the mean intensity of CD44, CD133, and CD166 CSC markers was higher in human metastatic CRC tissues than in nonmetastatic tissues (Figure 6, A and B). The migration rate and invasiveness of D-K-Ras-MT cells was higher than that of D-K-Ras-WT (D-K-Ras-MT cells mean = 90.057 pixel, 95% CI = 80.740 to 99.373 pixel; vs D-K-Ras-WT cells mean = 39.358 pixel; 95% CI = 35.169 to 43.547 pixel; $P = .03$) (Supplementary Figure 10, A and B, available online). Injection of D-K-Ras-MT cells into the spleen of mice resulted in liver metastasis in nine of 12 mice and lung metastasis in three of 12 mice, whereas none of the mice injected with D-K-Ras-WT cells developed metastasis (Figure 6C). Thus, oncogenic *K-Ras* induces distal metastasis of CRCs harboring *APC* mutation.

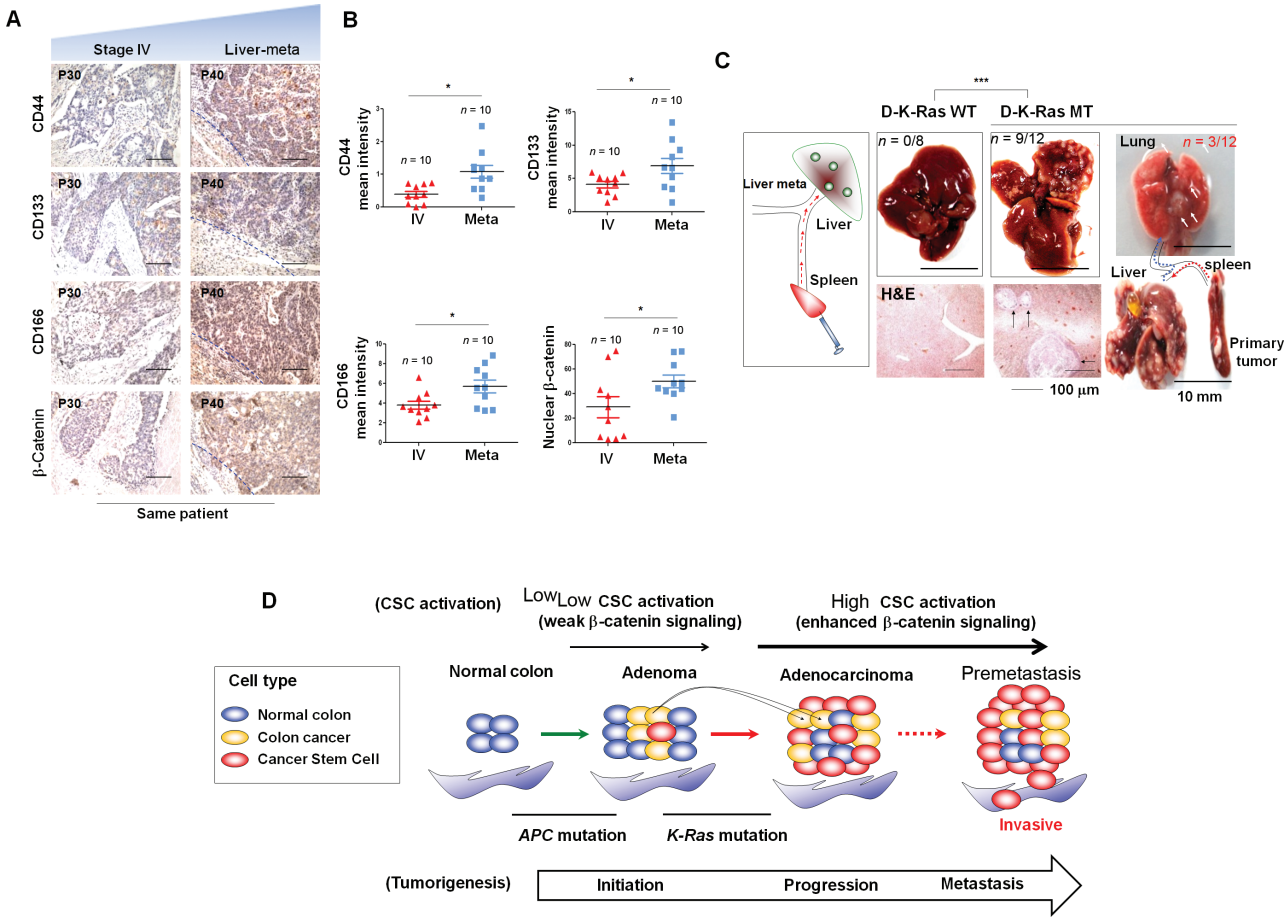

Figure 6. Oncogenic *K-Ras* induces metastasis of colorectal cancer cells carrying *APC* mutation. **A** and **B**) Paraffin sections from stage IV human adenocarcinoma and associated distal liver metastases (stage IV adenocarcinoma/metastatic tumor = 10:10) were subjected to immunohistological staining using antibodies against CD44, CD133, CD166, or β-catenin and quantified by Histo Quest software. Representative images were selected from at least three different fields. Data are shown as mean ± standard deviation for at least 10 independent specimens. $*P < .05$, two-sided *t* test. Scale bar = 200 μm. **C**) Nude mice were injected intrasplenically with D-K-Ras-WT (n = 8) or D-K-Ras-MT (n = 12) cells and grown for 8 weeks. After mice were killed, gross liver images were captured by an optical camera, and the tissues were subjected to hematoxylin and eosin (H&E) staining (**middle lower panel**; scale bar = 100 μm). Primary tumors were detected in the spleen, and liver metastases were evident in the mice injected with D-K-Ras-MT cells. Lung metastatic tumors were also observed in three of 12 mice injected with D-K-Ras-MT cells (**right panel**; scale bar = 10 mm. **D**) Genetic model of colorectal tumorigenesis involving both *APC* and *K-Ras* mutations. *APC* mutation is involved in the initiation of colorectal cancer and leads to adenoma. An additional *K-Ras* mutation at the early adenoma stage strongly enhances Wnt/β-catenin signaling as a result of ERK pathway activation through mutant K-Ras protein stabilization (Figure 5F) (22). Enhanced Wnt/β-catenin signaling induces an increase in the number of cancer stem cells (CSCs; **thick arrow**), leading to adenocarcinoma and further progression to metastasis.

Discussion

CSCs are involved in the progression and metastasis of various cancer types including CRC (2,5). Although mutation of *K-Ras* is known to play important roles in the progression and metastasis of tumors (8,20), its involvement in CSC-mediated tumorigenesis is poorly understood. The oncogenic *K-Ras* mutation induces stemness of CRC cells carrying an *APC* mutation, as shown by comparisons of sphere formation, transforming potential, chemoresistance, differentiation, and expression of stem cell markers between isogenic *APC* mutated CRC cells harboring either wild-type or mutant *K-Ras*. The activation of CSC by *K-Ras* mutations in CRC requires an additional *APC* mutation, as revealed by the induction of CD44, CD133, and CD166 in intestinal tumor tissues of $APC^{Min/+}$/$K\text{-}Ras^{LA2}$ double-mutant mice, but not in $K\text{-}Ras^{LA2}$ mice. The requirement for *APC* loss in the activation of CSC and tumor growth was supported by in vitro studies showing rescue of the sphere-forming capacity of RKO CRC cells harboring wild-type *APC* and *K-Ras* by transfection with truncated $APC^{1\text{-}777}$ construct and an additive increase in the sphere-forming capacity with coexpression of both $K\text{-}Ras^{V12}$ and $APC^{1\text{-}777}$. The progressive growth of tumors induced by mutation in both *APC* and *K-Ras* may be attributed to the activation of CSCs, as indicated by the marked enhancement of the expression of CD44, CD133, and CD166 in the mouse xenograft tumors induced by D-K-Ras-MT cells compared with those generated by D-K-Ras-WT cells. We further confirmed enhanced activation of CSCs by *APC* and *K-Ras* mutations by the induction of CSC markers in $APC^{Min/+}$/$K\text{-}Ras^{LA2}$ mice compared with $APC^{Min/+}$ or $K\text{-}Ras^{LA2}$ mice. The role of oncogenic *K-Ras* mutation in CSC activation and tumor formation was confirmed by the effects of knockdown of oncogenic K-Ras on CSC activation and xenograft tumor growth induced by D-K-Ras-MT cells. By microarray analyses, we also observed higher expression of CD44, CD133, and CD166 mRNA in *K-Ras* mutated CRC patient

tissues carrying mutant *APC* compared with those with wild-type *APC*. These data support a pathophysiological role for *APC* mutation in CSC activation in CRC with *K-Ras* mutations.

To determine the role of the ERK pathway in the enhancement of Wnt/β-catenin signaling by *APC* loss, we measured the effect of MEK inhibition in cells and xenograft tumors. This analysis indicated that the ERK pathway contributed to β-catenin activation in spheres and xenograft tumors derived from D-K-Ras-MT cells. This conclusion is further supported by studies showing the abrogation of the $APC^{Min/+}$ phenotype by p-ERK inhibition (29) and enhanced Wnt/β-catenin target gene activation in the presence of ERK pathway-activating *K-Ras* mutations (30,31). Although it is known that *APC* mutations occur during the early stages of carcinogenesis, initiating CRC, and oncogenic *K-Ras* mutations occur during the intermediate adenoma stages of colorectal tumorigenesis (8), the relationship between these mutations in intestinal tumorigenesis is poorly understood. In this study, we show that *K-Ras* mutation accelerates tumor growth through the activation of CSCs with preceding *APC* mutation. The role of Wnt/β-catenin signaling in the oncogenic *K-Ras*–induced activation of CSCs is supported by both in vitro and in vivo studies. We found that oncogenic *K-Ras* mutation both induced the expression of the CSC markers CD44, CD133, and CD166 and the nuclear localization of β-catenin in the presence of loss-of-function *APC* mutations.

Currently, it is not known why oncogenic *K-Ras* only induces the activation of CSCs and self-renewal activity in CRCs harboring *APC* mutations. Ras protein stabilization by *APC* loss is tightly associated with CRC in studies using both animal and human specimens (22). In this study, we further confirmed the stabilization of oncogenic K-Ras in $APC^{Min/+}$/$K\text{-}Ras^{LA2}$ double-mutant mice, which critically enhanced the expression of CSC markers and the growth of tumors. These results suggest that the initial activation of Wnt/β-catenin signaling by *APC* loss was further enhanced by the stabilization of the oncogenic K-Ras protein (Figure 5F). Although these data suggest that oncogenic K-Ras plays a role in CSC activation in CRCs harboring *APC* mutations, there are limitations in this study. Although the study was tested with human CRC patient tissues, it remains to be confirmed in a larger patient group because of the limited number of patient samples.

Overall, the progression and metastasis of CRC induced by *K-Ras* mutation occurs by initial activation of CSC by *APC* loss and further activation of Wnt/β-catenin signaling by subsequent activation of Ras-ERK signaling (Figures 5F and 6D). Considering the highly complex interaction between the Wnt/β-catenin and Ras-ERK pathways, a therapy targeting both pathways is an ideal approach for the treatment of colorectal cancer.

References

1. Jemal A, Siegel R, Ward E, et al. Cancer statistics, 2008. *CA Cancer J Clin*. 2008;58(2):71–96.
2. Pang R, Law WL, Chu AC, et al. A subpopulation of CD26+ cancer stem cells with metastatic capacity in human colorectal cancer. *Cell Stem Cell*. 2010;6(6):603–615.
3. Chaffer CL, Weinberg RA. A perspective on cancer cell metastasis. *Science*. 2011;331(6024):1559–1564.
4. Schepers AG, Snippert HJ, Stange DE, et al., Lineage tracing reveals Lgr5+ stem cell activity in mouse intestinal adenomas. *Science*. 2012;337(6095):730–735.
5. Dalerba P, Clarke MF. Cancer stem cells and tumor metastasis: first steps into uncharted territory. *Cell Stem Cell*. 2007;1(3):241–242.
6. O'Brien CA, Pollett A, Gallinger S, Dick JE. A human colon cancer cell capable of initiating tumour growth in immunodeficient mice. *Nature*. 2007;445(7123):106–110.
7. Vermeulen L, De Sousa EMF, van der Heijden M, et al. Wnt activity defines colon cancer stem cells and is regulated by the microenvironment. *Nat Cell Biol*. 2010;12(5):468–476.
8. Kinzler KW, Vogelstein B. Lessons from hereditary colorectal cancer. *Cell*. 1996;87(2):159–170.
9. Fearon ER, Vogelstein B. A genetic model for colorectal tumorigenesis. *Cell*. 1990;61(5):759–767.
10. van de Wetering M, Sancho E, Verweij C, et al. The beta-catenin/TCF-4 complex imposes a crypt progenitor phenotype on colorectal cancer cells. *Cell*. 2002;111(2):241–250.
11. Salic A, Lee E, Mayer L, Kirschner MW. Control of beta-catenin stability: reconstitution of the cytoplasmic steps of the wnt pathway in Xenopus egg extracts. *Mol Cell*. 2000;5(3):523–532.
12. Logan CY, Nusse R. The Wnt signaling pathway in development and disease. *Annu Rev Cell Dev Biol*. 2004;20:781–810.
13. Korinek V, Barker N, Moerer P, et al. Depletion of epithelial stem-cell compartments in the small intestine of mice lacking Tcf-4. *Nat Genet*. 1998;19(4):379–383.
14. Brabletz S, Schmalhofer O, Brabletz T. Gastrointestinal stem cells in development and cancer. *J Pathol*. 2009;217(2):307–317.
15. Lewis A, Segditsas S, Deheragoda M, et al., Severe polyposis in Apc(1322T) mice is associated with submaximal Wnt signalling and increased expression of the stem cell marker Lgr5. *Gut*. 2010;59(12):1680–1686.
16. Li J, Chen B. Oct4 was a novel target of Wnt signaling pathway. *Mol Cell Biochem*. 2012;362(1–2):233–240.
17. Janssen KP, Alberici P, Fsihi H, et al. APC and oncogenic KRAS are synergistic in enhancing Wnt signaling in intestinal tumor formation and progression. *Gastroenterology*. 2006;131(4):1096–1109.
18. Wood LD, Parsons DW, Jones S, et al. The genomic landscapes of human breast and colorectal cancers. *Science*. 2007;318:1108–1113.
19. Mani SA, Guo W, Liao MJ, et al. The epithelial-mesenchymal transition generates cells with properties of stem cells. *Cell*. 2008;133(4):704–715.
20. Nash GM, Gimbel M, Shia J, et al. KRAS mutation correlates with accelerated metastatic progression in patients with colorectal liver metastases. *Ann Surg Oncol*. 2010;17(2):572–578.
21. Kemper K, Grandela C, Medema JP. Molecular identification and targeting of colorectal cancer stem cells. *Oncotarget*. 2010;1(6):387–395.
22. Jeong WJ, Yoon J, Park JC, et al. Ras stabilization through aberrant activation of Wnt/beta-catenin signaling promotes intestinal tumorigenesis. *Sci Signal*. 2012;5(219):ra30.
23. Moon BS, Kim HY, Kim MY, et al. Sur8/Shoc2 involves both inhibition of differentiation and maintenance of self-renewal of neural progenitor cells via modulation of extracellular signal-regulated kinase signaling. *Stem Cells*. 2011;29(2):320–331.
24. Yun J, Rago C, Cheong I, et al., Glucose deprivation contributes to the development of KRAS pathway mutations in tumor cells. *Science*. 2009;325(5947):1555–1559.
25. Vermeulen L, Todaro M, de Sousa Mello F, et al. Single-cell cloning of colon cancer stem cells reveals a multi-lineage differentiation capacity. *Proc Natl Acad Sci U S A*. 2008;105(36):13427–13432.
26. Yoon J, Koo KH, Choi KY. MEK1/2 inhibitors AS703026 and AZD6244 may be potential therapies for KRAS mutated colorectal cancer that is resistant to EGFR monoclonal antibody therapy. *Cancer Res*. 2011;71(2):445–453.
27. Oudejans JJ, Slebos RJ, Zoetmulder FA, Mooi WJ, Rodenhuis S. Differential activation of ras genes by point mutation in human colon cancer with metastases to either lung or liver. *Int J Cancer*. 1991;49(6):875–879.
28. Todaro M, Alea MP, Di Stefano AB, et al., Colon cancer stem cells dictate tumor growth and resist cell death by production of interleukin-4. *Cell Stem Cell*. 2007;1(4):389–402.
29. Lee SH, Hu LL, Gonzalez-Navajas J, et al. ERK activation drives intestinal tumorigenesis in Apc(min/+) mice. *Nat Med*. 2010;16(6):665–670.

30. Horst D, Chen J, Morikawa T, et al. Differential WNT activity in colorectal cancer confers limited tumorigenic potential and is regulated by MAPK signaling. *Cancer Res*. 2012;72(6):1547–1556.
31. Singh K, Deshpande P, Li G, et al. K-RAS GTPase- and B-RAF kinase-mediated T-cell tolerance defects in rheumatoid arthritis. *Proc Natl Acad Sci U S A*. 2012;109(25):E1629–1637.

Funding

This work was supported by grants from the National Research Foundation (NRF) funded by the Ministry of Education, Science, and Technology of Korea (the Mid-career Researcher Program; 2012–010285), Translational Research Center for Protein Function Control (2009-0083522), and Stem Cell Research Project (2010-0020235). W. J. Jeong was supported by grants (NRF-2013R1A6A3A01028062), and B. S. Moon, J. Park were supported by a BK21 studentship from the NRF.

Notes

We thank Professor Jae-Gahb Park for providing raw microarray data.

Affiliations of authors: Department of Biotechnology (B-SM, W-JJ, JP, K-YC), Translational Research Center for Protein Function Control (B-SM, W-JJ, JP, DSM, K-YC), and Department of Internal Medicine and Institute of Gastroenterology, College of Medicine (TIK), Yonsei University, Seoul, Korea; Department of Molecular Biology, College of Natural Science, Pusan National University, Pusan, Korea (DSM).